

Supplementary Information

Bubble-bubble pinch-off in symmetric and asymmetric microfluidic expansion channels for ordered foam generation

Daniel Vecchiolla, Vidya Giri, and Sibani Lisa Biswal*

Department of Chemical and Biomolecular Engineering, Rice University, Houston, TX, USA

*Corresponding author: E-mail: biswal@rice.edu

Supplementary Video 1: High density monodisperse pinch-off (12 mL h⁻¹ and 1050 mbar, Ca ≈ 0.074, PDI of 5.8% ± 0.1%, bubble radius of 59.7 μm) at 30075 fps in a symmetric expansion (45° walls). Still images for Fig. 2a-h are every 2 frames of video playback from 5 to 19 seconds. Still images for Fig. 7a-e are every 4 frames of video playback from 8 to 24 seconds. Fig. 7f shows the resultant bidisperse foam in the wide collection channel.

Supplementary Video 2: Low density monodisperse pinch-off (22 mL h⁻¹ and 1125 mbar, Ca ≈ 0.096, PDI of 4.9% ± 0.2%, bubble radius of 38.5 μm) at 50000 fps in a symmetric expansion (45° walls). Still images for Fig. 7i-v are every 4 frames of video playback from 18 to 34 seconds. Fig. 7vi shows the resultant bidisperse foam in the wide collection channel.

Supplementary Video 3: High efficiency bidisperse pinch-off (16 mL h⁻¹ and 1000 mbar, Ca ≈ 0.074, PDI ≤ 4% for each fragmented band individually, bubble radius of 53.1 μm) at 27027 fps (recorded at 54054 fps) in an asymmetric expansion (an upper 45° wall and a lower 60° wall). The fragmented bubble size ratio $\theta = 1.50$ corresponds to $\eta = (\theta - 1) / (\theta_{\max} - 1) = 0.83$ with $\theta_{\max} \approx 1.60$ as demonstrated in Fig. S3. Fig. 11b shows the resultant tridisperse foam in the wide collection channel.

Fig. S1: High density polydisperse pinch-off (8 mL h⁻¹ and 925 mbar, Ca ≈ 0.055, PDI of 10.4% ± 1.4%, bubble radius of 67.5 μm). Fig. 6a shows the resultant polydisperse foam in the wide collection channel. The time interval between images is 0.13 ms. Scale bars are 100 μm.

Fig. S2: Low density polydisperse pinch-off (20 mL h⁻¹ and 1000 mbar, Ca ≈ 0.078, PDI of 8.8% ± 0.3%, bubble radius of 39.4 μm). Fig. 6b shows the resultant polydisperse foam in the wide collection channel. The time interval between images is 0.04 ms. Scale bars are 100 μm.

Fig. S3: Schematic comparing the ratio of the tangents of the expansion walls with the expansion width ratio.

Fig. S4: Schematic of the misalignment between the centerlines of the narrow channel and the wide asymmetric channel.

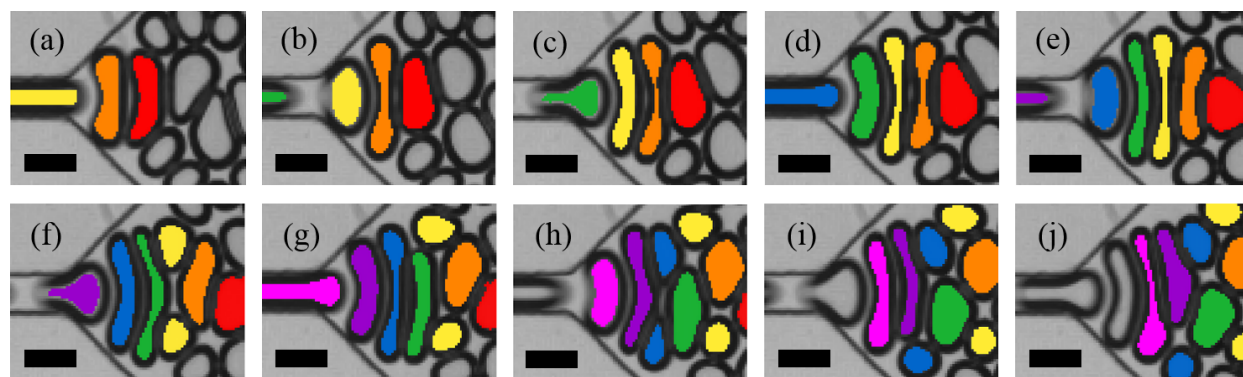


Fig. S1: Following a high density symmetric pinch-off event, (a-c) a “skipped” pinch-off event where the elongated (orange) bubble does not split, contrary to the optimal every other bubble pattern. The normal forces of the surrounding bubbles were reduced by the nearly complete retracting of the downstream confining (red) bubble as well as the thinning of the upstream (yellow) confining bubble by the incoming (green) bubble. (c-d) Asymmetric thinning of the central (yellow) bubble due to the bottom-heavy distribution of the (orange) wall bubble. The roles of the orange and yellow bubble have shifted from “pinched” and “pincher” to wall and pinched bubble respectively. (e-f) Asymmetric pinch-off with the bigger fragmented (yellow) bubble at top resulting from the initial thinning rather than the current top-heavy distribution of the (orange) wall bubble. (g-h) Asymmetric thinning and pinch-off of the elongated (blue) bubble due to off-center positioning of the (green) wall bubble as a result of (yellow) fragmented bubble traffic (i.e. the size disparity in the yellow fragmented bubbles causes the green pincher bubble to flow downwards along the path of least resistance). (i-j) Asymmetric pinching due to uneven retracting from bottom to top and off-center positioning of the (purple) wall bubble resulting from the location of the fully retracted (green) bubble below the centerline of the expansion inlet. (j) The resulting thinning of the upstream (pink) bubble leads to asymmetric pinch-off (not shown) with the respective daughter bubble sizes inverted in relation to the preceding pinch-off event

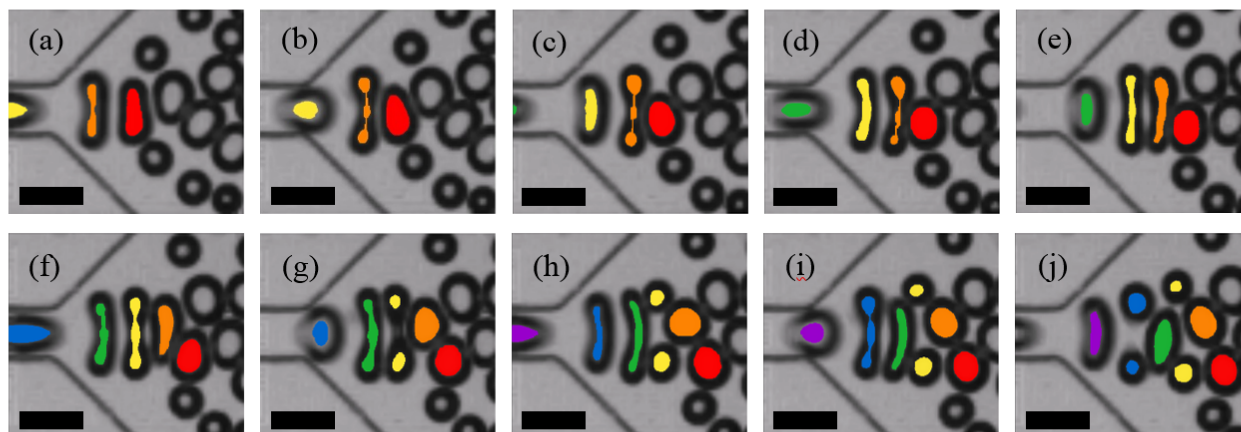


Fig. S2: Similar phenomena as Fig. S1. Following a low density symmetric pinch-off event, (a-d) a “skipped” pinch-off event where the elongated (orange) bubble does not split, contrary to the optimal every other bubble pattern. The normal forces of the surrounding bubbles were reduced by the nearly complete retracting of the downstream confining (red) bubble prior to the upstream (yellow) confining bubble advancing into close proximity with the central (orange) bubble. (e-h) Asymmetric thinning and pinch-off of the elongated (yellow) bubble due to uneven retracting of the (orange) wall bubble from bottom to top resulting from the location of the fully retracted (red) bubble below the centerline of the expansion inlet. (h-j) Asymmetric thinning and pinch-off of the elongated (blue) bubble due to off-center positioning of the (green) wall bubble as a result of (yellow) fragmented bubble traffic (i.e. the size disparity in the yellow fragmented bubbles causes the green pincher bubble to flow downwards along the path of least resistance). (j) The respective sizes of the two pairs of daughter bubbles are inverted and the positioning of the bubbles matches with Fig. S1h. Note: a “skipped” pinch-off event is not a requirement for initiating asymmetric pinch-off.

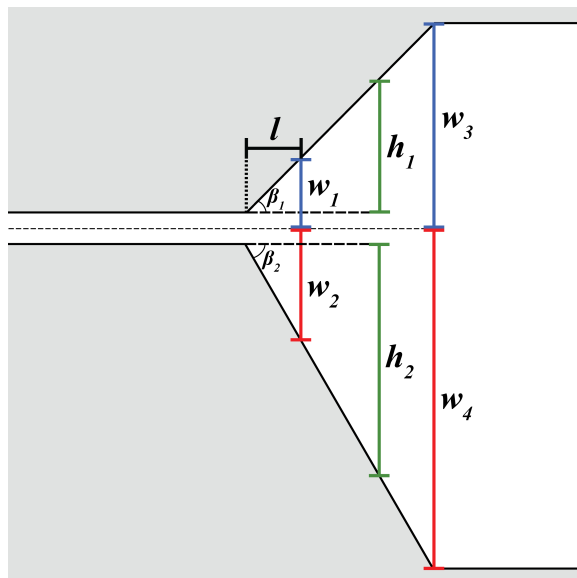


Fig. S3: Schematic comparing the ratio of the tangents of the expansion walls with the expansion width ratio. As derived in Supplementary Note 2 of Rosenfeld et al.,¹ geometric arguments show that strain rate is proportional to the tangent of the expansion wall angle. The fragmented bubble size ratio θ thus scales with the ratio of the tangents of the wall angles in an asymmetric expansion. For our design with $\beta_1 = 45^\circ$ and $\beta_2 = 60^\circ$, $\tan(\beta_2)/\tan(\beta_1) = h_2/h_1 = 1.732$. However, the nonzero width of the narrow channel upstream ($w_c \approx 70 \mu\text{m}$) causes the expansion width ratio (the ratio of the perpendicular distances from the centerline of the narrow channel to the expansion walls) to be lower for a finite expansion. At the end of the expansion ($\approx 560 \mu\text{m}$ from the inlet), the expansion width ratio is $w_4/w_3 = 1.69$ and near the beginning of the expansion ($50 \mu\text{m}$ from the inlet, not shown above) the local expansion width ratio is only about 1.43. The expansion length l is the distance within the expansion a bubble travels along the narrow channel centerline upon reaching a stagnation point and undergoing pinch-off.² Taking an expansion length l as roughly $160 \mu\text{m}$ or below, the true maximum size ratio is $\theta_{\max} \approx w_2/w_1 = 1.60$ as governed by the Hagen-Poiseuille equation.

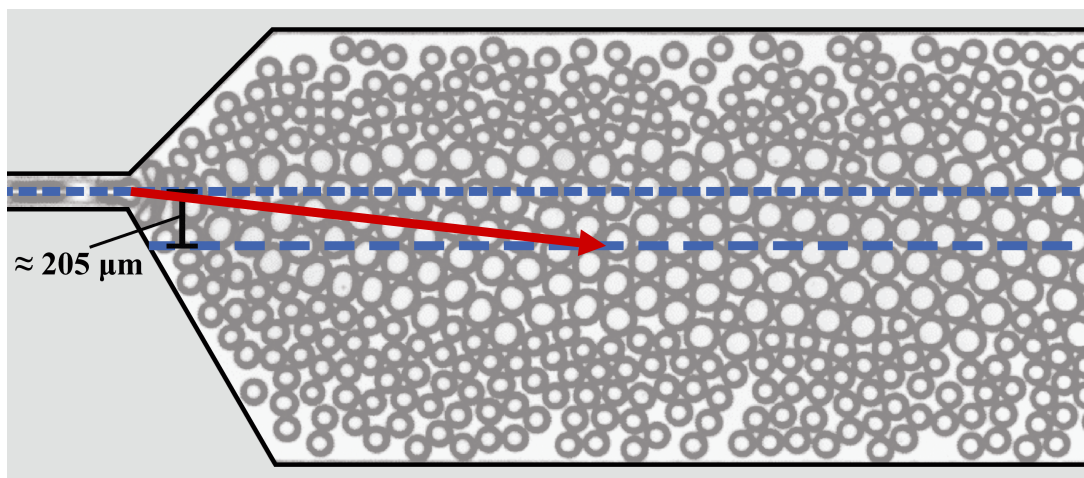


Fig. S4: Schematic of the misalignment between the centerlines of the narrow channel and the wide asymmetric channel ($\approx 205 \mu\text{m}$). The streamlines result in the bending of the single file template of bubbles due to the downward flow towards the collection channel centerline. In this slanted configuration, the contribution to fluidic resistance from the expansion is reduced, and the monodisperse intact bubbles more symmetrically pinch-off the central bubble. The misalignment is overlaid on the still image from Fig. 13f of low efficiency pinch-off (14 mL h^{-1} and 1075 mbar , $\text{Ca} \approx 0.076$, average PDI of 4.5%, bubble radius of $66.4 \mu\text{m}$, $\theta = 1.08$ corresponding to $\eta = 0.13$). For comparison, the misalignment for a $1000 \mu\text{m}$ channel instead of a $1600 \mu\text{m}$ would be roughly $125 \mu\text{m}$ (or almost 40% less), which should improve overall efficiencies.

References

1. L. Rosenfeld, L. Fan, Y. Chen, R. Swoboda, and S. K. Y. Tang. *Soft Matter*, 2014, **10**, 421-430.
2. W. Lee, L. M. Walker and S. L. Anna, *Phys. Fluids*, 2009, **21**, 032103.